

Geophysical Research Letters

RESEARCH LETTER

10.1029/2018GL080463

Key Points:

- Variations of annual temperature for tropical land regions have become much more spatially synchronized in recent decades
- Stronger spatial coherence of tropical land temperature tends to occur in warm phases of the oceanic Pacific Decadal Oscillation
- Climate models suggest that the linkage between PDO state and coherence of tropical land temperature can adjust under global warming

Supporting Information:

- Supporting Information S1

Correspondence to:

S. Piao,
slpiao@pku.edu.cn

Citation:

Yang, H., Piao, S., Huntingford, C., Peng, S., Ciais, P., Chen, A., et al. (2019). Strong but intermittent spatial covariations in tropical land temperature. *Geophysical Research Letters*, 46, 356–364. <https://doi.org/10.1029/2018GL080463>







Received 13 SEP 2018

Accepted 22 DEC 2018

Accepted article online 28 DEC 2018

Published online 13 JAN 2019

Strong but Intermittent Spatial Covariations in Tropical Land Temperature

Hui Yang¹ , Shilong Piao¹ , Chris Huntingford² , Shushi Peng¹ , Philippe Ciais^{1,3}, Anping Chen⁴ , Guiyun Zhou⁵, Xuhui Wang^{1,3}, Mengdi Gao¹, and Jakob Zscheischler^{6,7,8} 

¹Sino-French Institute for Earth System Science, College of Urban and Environmental Sciences, Peking University, Beijing, China, ²Centre for Ecology and Hydrology, Benson Lane, Wallingford, UK, ³Laboratoire des Sciences du Climat et de l'Environnement, CEA CNRS UVSQ, Gif-sur-Yvette, France, ⁴Department of Forestry and Natural Resources, Purdue University, West Lafayette, IN, USA, ⁵School of Resources and Environment, University of Electronic Science and Technology of China, Chengdu, China, ⁶Institute for Atmospheric and Climate Science, ETH Zurich, Zurich, Switzerland, ⁷Climate and Environmental Physics, University of Bern, Bern, Switzerland, ⁸Oeschger Centre for Climate Change Research, University of Bern, Bern, Switzerland

Abstract Surface temperature variations across the tropics exhibit different levels of spatial coherence, yet this is poorly characterized. Years of high temperature anomalies occurring simultaneously across large geographical regions have the potential to adversely impact food production and societal well-being. Using cluster analysis of correlations between extensive temperature measurements from the last six decades, we find a major change occurs in the late 1970s. Two spatial clusters merge to a single dominant one, and therefore, warmer years are experienced at the same time across most tropical land regions. Noting this change occurs at the same time as the Pacific Decadal Oscillation shifts a warm phase, we investigate this potential driver by a range of coupled ocean-atmosphere-land climate models. These simulations verify that stronger spatial tropical land temperature coherence tends to occur in Pacific Decadal Oscillation warm phases, although model differences exist in projections of how climate change may modulate this dependence.

Plain Language Summary Recent increasing surface temperature variations significantly enhance weather extremes and exacerbate food production and societal well-being. Adverse impacts of high temperature variations could be further aggravated when fluctuations of annual temperature are spatially coherent. Compared to isolated weather disasters, simultaneous co-occurrences of events may cause much broader damages and impair mitigation capacity. Yet it is unclear how temperature covaries across different regions, and if covariation strength is changing. Using cluster analysis of correlations between gridded temperature anomalies over the last six decades, we demonstrate increasing spatial coherence in temperature interannual variability. At the late 1970s, two spatial clusters merged into one dominant cluster covering tropical land regions. Stronger spatial temperature coherence tends to occur in Pacific Decadal Oscillation warm phases, although climate change may modulate this dependence.

1. Introduction

Changes in the characteristics of extreme climate events may cause a significant impact on ecosystems and society, especially when occurring in conjunction with general background global warming (Meehl & Claudia, 2004). Understanding the features of year-to-year variations of surface temperature (T) enables better preparation for any temperature extremes. Analysis of the climate system has enabled significant progress to be made in understanding the magnitude of fluctuations in annual temperature and the associated severity of regional extremes (Huntingford et al., 2013; Rahmstorf & Coumou, 2011). However, much less research has been undertaken to characterize degrees of spatial coherence in temperature variations between different regions. Large spatial coherence in temperature variations implies any adverse impacts of weather extremes can occur over large geographical domains at the same time. Heat waves occurring simultaneously over many locations, compared to isolated events, can have a much broader impact on ecosystems and human society. This can include enhanced forest mortality, exacerbated food production shortages, increased heat-related illnesses, and enlarged economic losses (Battisti & Naylor, 2009; Chavez et al., 2015). Furthermore, the transfer of mitigation in risk of extremes between regions and countries

will be impaired if they need to cope with concurrent extreme events (IPCC, 2012; Wilhelmi et al., 2004). An improved understanding of the extent, drivers, and possible changes in the spatial coherence of annual temperature variability, therefore, is essential for better adaptation planning to climate change and related detrimental impacts. Specifically, research is needed to identify the geographical boundaries of where annual anomalies in temperature vary similarly; to investigate whether such spatial connections have changed over time; and to explore whether further changes can be expected in spatial temperature coherence under future elevated atmospheric greenhouse gas concentrations.

K-means clustering statistical analysis (Arthur & Vassilvitskii, 2007) allows characterization of the spatial features of temperature interannual variability (IAV). We apply this cluster analysis to the Climate Research Unit (CRU) gridded air temperature data (Harris et al., 2014), which is based on the collation of direct temperature measurements from around the world. The statistical method partitions the CRU-based grid cells into different clusters, based on the similarity of their temperature annual variation. Each grid cell is assigned either to a cluster, or “outliers.” Within each cluster, grid-cell temperature IAV is significantly positively correlated. We calculate such spatial clustering patterns in three periods: years 1950–1976, 1977–1998, and 1999–2015. These time periods are selected here because they correspond to the observed regime shifts in the Pacific Decadal Oscillation (PDO), and there is significant evidence that geographical features of tropic land temperatures are strongly influenced by oceanic state (D’Arrigo et al., 2005). PDO has shifted twice recently, from a cold to a warm phase around 1976–1977 and back to a cold phase around 1998–1999 (Yeh et al., 2011). Our findings, including statistically based linkages to oscillations in the oceans, are further investigated in a more mechanistic framework by analysis of a large set of coupled climate models (Taylor et al., 2012).

2. Materials and Methods

2.1. Experimental Design

For our analysis of spatial coherence in land temperatures, we assess both observation-based data and General Circulation Model (GCM) outputs, and the latter for both preindustrial and abrupt $4 \times \text{CO}_2$ concentration scenarios. For the CRU data, we detrend annual temperature time series by removing the linear trend (least-squares fitting) over years and for each pixel. We use the statistical tool *K*-means clustering (see supporting information Text S1 for details) to partition global land grid cells into individual clusters. This is based on the values of correlation between different points and for temperature IAV. The clustering is performed for the three periods of 1950–1976, 1977–1998, and 1999–2015. In addition, to understand general changes, we use the spatial pattern of the clustering analysis for period 1950–1976 to define geographical masks. We calculate the area-weighted annual temperature within the first two cluster-based masks and assess how these temperatures and their difference then evolves for years beyond 1976.

Our application of climate simulations to support observation-based findings is as follows. We use 33 GCMs in the Coupled Model Intercomparison Project Phase 5 (CMIP5) database, corresponding to the preindustrial scenario, and a further 20 GCMs under the abrupt $4 \times \text{CO}_2$ scenario (Table S1). For understanding of potential oceanic drivers of land coherence change, we identify the PDO warm and cold phases for each GCM by the statistical climate regime shift test (Tables S2 and S3). This statistical test (Rodionov, 2004) is used to diagnose the change points (between PDO warm and cold phases) in oceanic temperature time series, and parameter cutoff length l (the minimum length of climate regimes) and probability level p are set to 10 and 0.05, respectively. With these parameters, the mean of PDO phase lengths diagnosed by statistical test is 18.4 years. During each of these periods identifying PDO phase, for each GCM simulation and scenario, we apply the same *K*-means clustering method to the gridded land temperature anomalies. From this, we calculate the fractional coverage of the largest cluster in tropics, as a percentage of the total tropical land surface, dependent on PDO phase, and as presented in Figures 3a and 3b.

2.2. Gridded Temperature Data Sets

Gridded temperature data used in this study include the data sets derived from observation and reanalysis estimates. Observation-based gridded temperature with a spatial resolution of $0.5^\circ \times 0.5^\circ$ over the global land surface is from CRU TS v4.00 data set. This product provides monthly air temperature during the period 1901–2015 inclusive, which are interpolated from meteorological station measurements. The alternative

four climate data sets include (I) Berkeley Earth Surface Temperature (Berkeley; Rohde et al., 2013) with a spatial resolution of $1^\circ \times 1^\circ$; (II) the European Center for Medium-Range Weather Forecast Reanalysis of the 20th century (Poli et al., 2016) with a spatial resolution of $0.5^\circ \times 0.5^\circ$; (III) the National Center for Environmental Prediction/National Center for Atmospheric Research Reanalysis 1 (Kalnay et al., 1996) with a spatial resolution of $2.5^\circ \times 2.5^\circ$; and (IV) the Global Soil Wetness Project Phase 3 with a spatial resolution of $0.5^\circ \times 0.5^\circ$.

2.3. Air Temperature and Sea Temperature From GCMs

We used simulations of 33 GCMs under the CMIP5 (Taylor et al., 2012). All the models provide simulations under preindustrial radiative forcing, and 23 models provide simulations under abrupt CO_2 forcing. For abrupt $4 \times \text{CO}_2$ experiment, 20 GCM outputs (except GISS-E2-H, GISS-E2-R, and Inmcm4) were used when mean global temperatures (ocean and land) exceed 3°C above preindustrial warming level and are transitioning to temperature stabilization (Figure S17). We used the monthly outputs of near-surface air temperature and sea surface temperature (SST) for the period 1901–2100, the latter was used to calculate PDO index. A brief summary of the main characteristics of the models is presented in Table S1.

2.4. PDO and NINO3.4 Index

The PDO is defined by the leading Empirical Orthogonal Function (EOF) of monthly SST anomalies over the North Pacific ($20^\circ\text{--}70^\circ\text{N}$, $110^\circ\text{E--}100^\circ\text{W}$). We used the historical monthly PDO index (1950–2015), which was downloaded from <http://jisao.washington.edu/pdo/PDO.latest> (Mantua et al., 1997; Zhang et al., 1997). Following their calculation, we then calculated the monthly PDO index from simulated SST from each of the CMIP5 models under “picontrol” and “abrupt4 $\times \text{CO}_2$ ” scenarios. The simulated SST anomalies at each grid point are obtained by subtracting both the local climatological annual cycle and the globally averaged SST. The spatial pattern of the PDO is computed by multiple SST anomalies at each grid point over the global oceans and the associated first principal component time series. The PDO spatial pattern and the first principal component record from CMIP5 models are displayed in Figure S11 (under preindustrial scenario) and Figure S12 (under abrupt4 $\times \text{CO}_2$). Warm phase of the PDO ($\text{PDO} > 0$) coincides with positive SST anomalies along the west coast of North America and negative SST anomalies in central and western North Pacific. Note that the cold phase of the PDO ($\text{PDO} < 0$) is also associated with positive SST anomalies across the central and eastern tropical Pacific. Previous independent studies find evidence that a regime shift from cold to warm PDO modes took place in 1976, whereas a shift from warm to cold PDO modes occurred in 1998 (Mantua & Hare, 2002).

NINO3.4 SST index was identified as being the most El Niño-Southern Oscillation (ENSO) representative. The NINO3.4 index in this study was calculated by SST measurements between $5^\circ\text{N--}5^\circ\text{S}$ and $120^\circ\text{--}170^\circ\text{W}$. SST measurements come from the Met Office Hadley Centre SST data set (HadISST; Rayner et al., 2003). According to the definition of ENSO events (Trenberth, 1997), monthly NINO3.4 index should be smoothed by 5-month running mean. The smoothed NINO3.4 anomalies, which are above or below $\pm 0.4^\circ\text{C}$ and persist for at least six consecutive months, indicate El Niño and La Niña.

3. Results

3.1. Cluster Analysis of Observation-Based Temperature Data

For the first period 1950–1976, tropical land temperature variations separate broadly into two distinct clusters, named “I” and “II”, shown as red and blue, respectively, in Figure 1a. Cluster I covers eastern Africa and Southeast Asia (23% of tropical land area). Cluster II covers most of the Amazon, western and southern Africa, and Australia (35% of tropical land area). For the period of 1977–1998, these two clusters broadly converge into a single cluster (Figure 1b). That is, annual temperature varies in synchrony in most tropical land regions during those years. This includes northern South America, most of Africa, Southeast Asia, and northern Australia. For period of 1999–2015, temperature IAV in Amazonia, western and central Africa, and Southeast Asia is still coherent (Figure 1c; red), but Australia is reclassified back in to another cluster (Figure 1c; blue). Tropical fractional areas for the clusters in each three periods are presented in Figure 1d. We provide additional information on the cluster features in the supporting information. The center of any of our clusters (mean temperature anomaly) is an overall summary of any particular cluster. We show that

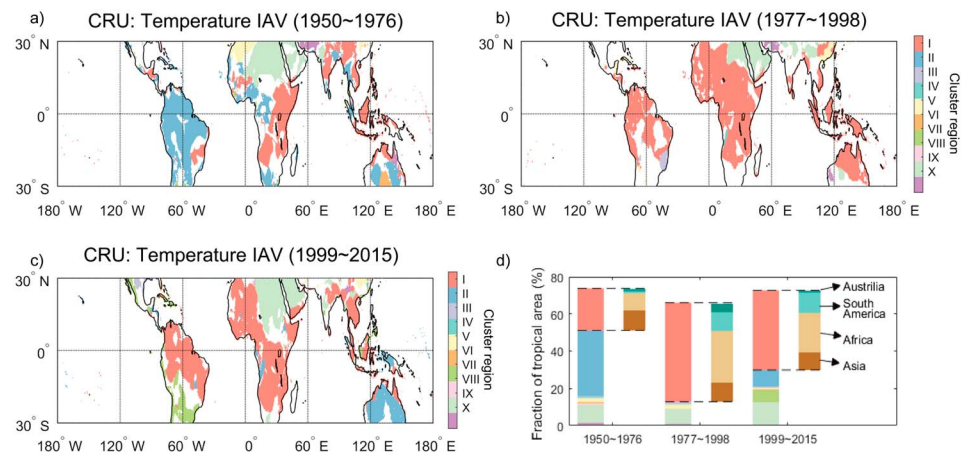


Figure 1. Spatial patterns of clusters characterized by the correlations of interannual variability in local temperature anomalies. Shown for the tropical regions (30°N–30°S) and for the periods (a) 1950–1976; (b) 1977–1998; and (c) 1999–2015. Grid cells are colored according to the cluster to which they are assigned. White cells are defined as outliers, which can be regarded as any remaining noise. (d) Fractional area of tropical regions (30°N–30°S) sorted in to different clusters. Fractional area of cluster I (red) is split in to values for four different continents of Asia, Africa, South America, and Australia. CRU = Climate Research Unit; IAV = interannual variability.

the time series of these, along with both maps and figures showing the spread of the correlations between different points in the clusters and these centers (Figure S1 and Text S2).

Our finding that annual temperature variations for tropical regions have become more spatially consistent is confirmed by additional analyses. First, we verify that this result is independent of window length for performing clustering analysis. Different time-window lengths (3×20 - or 2×30 -year) are tested (Figures S2 and S3), showing similar more recent merging of dominant clusters. We also apply the cluster analysis for the entire period 1950–2015 (Figure S4a). When analyzing the distribution of correlations between local points in cluster I and their cluster center, we observe that correlations during the more recent periods become higher (Figure S4b). This provides further evidence of recent increases in coherency of tropical temperature anomalies (Text S3). Second, we confirm the robustness of our result as independent of the temperature data used (Figure S5). This is by repeating clustering analysis with (I) Berkeley, (II) European Center for Medium-Range Weather Forecast Reanalysis of the 20th century, (III) National Center for Environmental Prediction/National Center for Atmospheric Research reanalysis, and (IV) Global Soil Wetness Project Phase 3 temperature estimates. Third, we confirm our finding is not an artifact of the interpolation techniques or numerical climate reanalysis models used in gridded data temperature construction from point weather station measurements. We instead calculate correlations of temperature measurements directly from individual meteorological stations across tropical regions (Harris et al., 2014). We again find correlations have increased since 1977 (Figure S6). Fourth, we verify the increased spatial coherence is not caused by recent decreases in number of available tropical meteorological stations (Figure S7). We test this by rebuilding the gridded CRU temperature data and adopting their interpolation approach but instead only using the 1,032 stations available for the full period 1950 to 2015 (Harris et al., 2014; Mitchell & Jones, 2005; New et al., 1999, 2000). Fifth, we show recent increased coherence of temperature variability is independent of number of clusters defined by the *K*-means algorithm. Instead of selecting the optimal number of clusters (“elbow method”, Text S1), we force the number of clusters (up to five) in the region 40°S–40°N. Broadly, two dominant clusters remain as initially present, converging to one after 1976 (Figure S8). Sixth, we also assess the temporal changes in correlation coefficients between the centers of clusters I and II. Now we derive clusters I and II from the spatial cluster analysis for the first period 1950–1976 only and keep these boundaries invariant until present day. Correlations between the cluster centers of the two predefined regions (from 1950–1976) have substantially increased in more recent years (Figure S9). This provides additional confirmation that the temperature variations for these two initial regions, which cover most tropical land regions, have become spatially

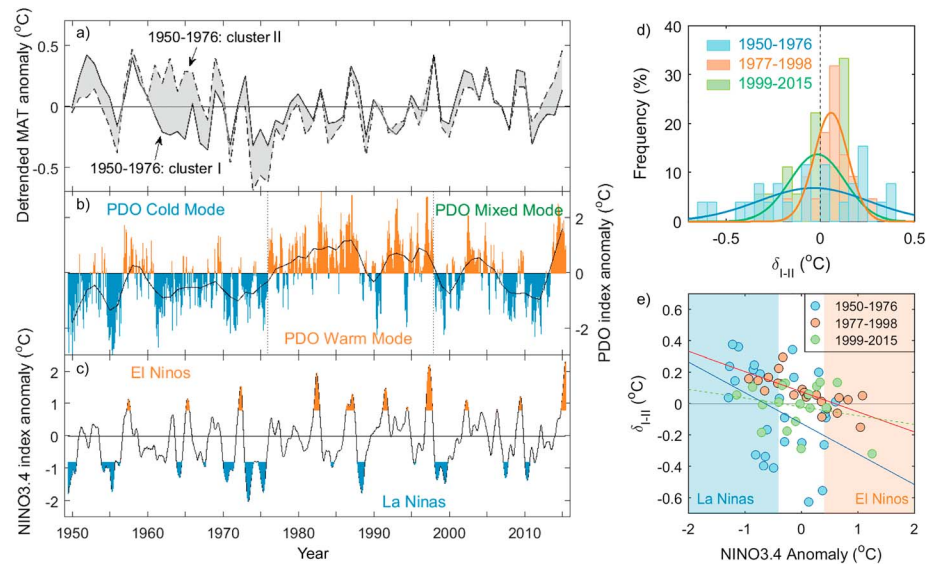


Figure 2. Temporal variation in the regional temperature over the tropics, and PDO, NINO3.4 SST index anomaly. (a) Changes in detrended area-weighted average of the temperature variations within cluster I (continuous black line) and cluster II (dashed black line). These two correspond to cluster regions I and II of Figure 1a. The gray shading shows the difference of temperature anomalies between these two clusters (δ_{I-II}). Changes in (b) monthly PDO index anomaly and (c) monthly NINO3.4 SST index anomaly (5-month filter) during the period 1950–2015. Positive anomalies greater than 0.4°C are shaded to indicate El Niño event, and negative anomalies less than -0.4°C indicate La Niña event. (d) The distribution of δ_{I-II} during the PDO cold (blue), warm (orange), and mixed (green) phases. (e) Values of δ_{I-II} versus NINO3.4 SST anomaly in PDO cold (1950–1976), warm (1977–1998), and mixed (1999–2015) phases. PDO = Pacific Decadal Oscillation; SST = sea surface temperature.

synchronized across one larger area. Finally, although providing less information than *K*-means clustering, we apply EOFs to temperature records as an alternative representation of their spatial coherence. The leading EOF of temperature variations shows a strong anticorrelated pattern of positive and negative values across the tropics for 1950–1976 but a more spatially uniform distribution for the 1977–1998 and 1999–2015 periods (Figure S10).

3.2. Potential Oceanic Forcing

We assess potential forcings for the observed increase in spatial coherence of tropical temperature IAV after the late 1970s. Within the spatial boundaries of clusters I and II derived from the clustering pattern for the first period 1950–1976 (Figure 1a), we calculate the area-weighted average temperature for each year of the entire period 1950–2015 (Figure 2a). As expected after 1976, the difference between the two clusters (called δ_{I-II} and with $|\delta_{I-II}|$ marked gray in Figure 2a) becomes generally smaller. There is much evidence that climate variability associated with the PDO and the ENSO phase strongly influences tropical land temperature variations (Evans et al., 2001). Hence, we add time series of the PDO and NINO3.4 SST index in Figures 2b and 2c, respectively, allowing comparison against time-evolving δ_{I-II} . For 1950–1976, the PDO is in a cold phase, during which coherence of temperature IAV between clusters I and II is weak. This is reflected in large δ_{I-II} (Figure 2a) and low correlation coefficient between the two cluster *T* anomalies ($r = 0.32$, $p = 0.11$). For 1977–1998, however, the PDO is in a warm positive phase, during which the mean temperatures in the two previous cluster regions (i.e., regions I and II, as defined during 1950–1976) are highly synchronized ($r = 0.92$, $p < 0.001$). Years 1977–1998 are when the two previous clusters converged into one with a merging of regions (Figure 1b). During period 1999–2015 (mixed PDO phase), PDO time series are short episodes of negative and positive values. Figure 2d shows the probability density functions of δ_{I-II} for the cold (1950–1976, blue), warm (1977–1998, orange), and mixed PDO phases (1999–2015, green). The distribution spread of divergence in temperature between clusters I and II, as quantified by the inter-quartile range in δ_{I-II} , during the cold phase of PDO is 0.46°C . This is more than twice that during the PDO warm phase, when it is 0.18°C .

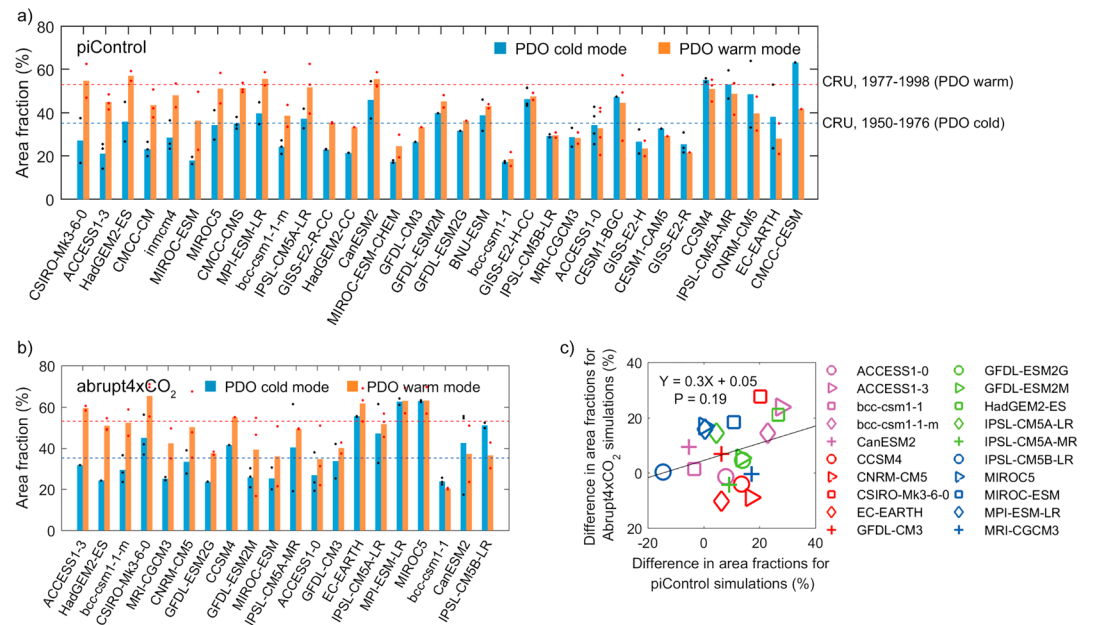


Figure 3. The mean area fraction (%) of tropical land cover (30°S–30°N) by the largest cluster with coherent features of temperature variations. (a) This is for 33 CMIP5 GCMs, based on the last 150 years of their preindustrial simulations (GCMs named on horizontal axis). Presented are values for GCM PDO warm and cold phases, and models are ranked in ascending order of the difference in area between these two values. Where more than one period is found in either state, histogram bars are mean values, and dots are individual values. For reference, dashed blue and red lines are area fraction of the largest cluster in tropics during the PDO cold phase (1950–1976; cluster II) and PDO warm phase (1977–1998; cluster I), based on the CRU data, as shown Figure 1d. (b) The same as (a) but based on the available abrupt $4 \times \text{CO}_2$ experiments. GCM outputs are used when mean global temperatures (ocean and land) are stabilized. (c) Modeled difference in fractional area between PDO warm and PDO cold under preindustrial scenario (differences based on (a) versus those under abrupt $4 \times \text{CO}_2$ scenario based on (b)). PDO = Pacific Decadal Oscillation; CRU = Climate Research Unit.

In general, there are more La Niña events during PDO cold phases and more El Niño events during PDO warm phases (Christensen et al., 2013). The SST anomalies for the peak of El Niño resembles that for the warm phase of PDO (and similarly La Niña resembles that for the cold phase of PDO). However, an ENSO event, or even the more persistent La Niña events, typically lasts only for 9–18 months, whereas PDO regimes generally persist for several years or decades (Newman et al., 2016). We investigate the linkage between NINO3.4 index and δ_{I-II} during the PDO cold, warm, and mixed phases (blue, red, and green circles, Figure 2e; periods as marked Figure 2b). Coherence of temperature IAV between clusters I and II shows a significant negative correlation with NINO3.4 index in both PDO cold ($r = -0.40, p < 0.05$) and warm phases ($r = -0.74, p < 0.05$), but not during the PDO mixed phases ($r = -0.22, p = 0.37$). However, also in Figure 2e, in general, there is much weaker spatial coherence of temperature anomalies during PDO cold phase, in either El Niño or La Niña years. For the PDO warm phase, regardless of the NINO3.4 index, we observe relatively high coherence, that is, $|\delta_{I-II}|$ is small.

3.3. Analysis of Coupled Climate Models

We use coupled ocean-atmosphere-land GCMs to assess further temperature coherence dependence on PDO, and whether this is affected by climate change from increasing atmospheric greenhouse gas concentrations. We again use cluster analysis for correlation coefficients between modeled annual temperature variations, now applied to GCM projections of tropical land temperature. Figures 3a and 3b present the mean fractional area of the largest cluster in tropical land regions. This is subdivided, according to which phase of PDO is modeled, and values presented for preindustrial conditions (Figure 3a) or for available GCMs modeling equilibrium conditions at $4 \times \text{CO}_2$ concentrations (Figure 3b). The patterns of the PDO and the typical duration of any phases are diagnosed from each GCM (Figures S11 and S12).

For preindustrial experiments, 22 out of 33 GCMs show that the geographical areas of the largest cluster with coherent temperature variations are more extensive during the PDO warm phases (Figure 3a). For the

$4 \times \text{CO}_2$ climate, a similar pattern emerges, with a high proportion of models (16 out of 20 GCMs) showing larger spatially coherent temperature variations during the PDO warm phase (Figure 3b). We then consider for the individual GCMs with both preindustrial and $4 \times \text{CO}_2$ simulations, the differences in each model of the largest cluster fractional area (PDO warm minus PDO cold periods) for preindustrial, versus the same quantity for abrupt $4 \times \text{CO}_2$ simulations. There is no significant relationship (Figure 3c). Hence, despite the similarities between Figures 3a and 3b, the dependence of tropical temperature coherence on PDO phase may change under the elevated CO_2 concentration, and including where for a few GCMs, the fractional differences have reversed under $4 \times \text{CO}_2$ (Figures 3a versus 3b).

In the supporting information, we present the clustering for the individual GCMs, to enable comparison to Figure 1. These are for each GCM, for different warm and cold PDO periods, and shown for preindustrial CO_2 concentrations (Figure S13) and $4 \times \text{CO}_2$ (Figure S14). The most general description is that there are similarities between cluster shapes in the GCMs, as found in recent measurements (i.e., Figure 1). However, distinct GCM differences do exist in some models, and tropics-PDO linkages are known to have difference between the CMIP5 models (Bellenger et al., 2014; Newman et al., 2016). This suggests a quite complex inter-GCM variation of spatial coherence of tropical temperature. Figures S13 and S14 again illustrate some GCMs (e.g., IPSL-CM5A-LR and CanESM2) reverse dominance in their largest cluster area (cold PDO periods vs. warm PDO periods) between preindustrial and $4 \times \text{CO}_2$ levels. However, even in these circumstances, some features of cluster extent and shape are retained between the two CO_2 levels (Figure S15).

4. Discussions and Conclusions

We use cluster analysis to verify that temperature variations across tropical South America, Africa, and Southeast Asia have changed during recent decades, becoming more spatially coherent. We identify a particular shift around 1976/1977, which is also a time when the PDO changed from cold to warm phase. GCMs generally support such a shift-dependence, with more than 65% of climate models having larger tropical spatial coherence of temperature variation in PDO warm phases. However, inter-GCM differences are large for some models. Interestingly, although a large fraction of model project increased spatial coherence of temperature from PDO cold to warm phases, many models do not capture the continental separation of clusters between South America and Africa which is evident in the observations for the PDO cold phases.

Our present study is predominantly statistically based. We hope that its findings will encourage more process-based investigations into the drivers of spatial coherence changes in tropical land temperature and any linkages to PDO state. Existing literature confirms the general finding that variation in midlatitude Pacific SSTs, and which are part of the defined PDO region, may modulate equatorial temperatures (or at least tropical SSTs). The Walker circulation has been long established as one possible process connecting oceanic state and land temperature (Julian & Chervin, 1978), as variation in this is strongly associated with tropical meteorological conditions. More recent research provides evidence of strong connections between PDO state and Walker circulation strength (Dong & Lu, 2013), including how SST variations adjust its circulation strength (Liu & Alexander, 2007; Newman et al., 2016). Such circulation changes alter the transport of heat, either directly through the atmosphere (Farneti, 2017; Hazeleger et al., 2005) or by surface wind changes adjusting ocean currents, the latter impacting on the equatorward advection of temperature (Miller & Schneider, 2000). We suggest these references can provide a starting point toward a better mechanistic understanding of our findings, including if any circulation-related large-scale thermal teleconnections adjust coherence levels. In addition, future analyses could also include determining whether PDO state adjusts spatial coherence in tropical precipitation, adding to the general evidence that Pacific oceanic multi-decadal dynamics may modulate tropical land precipitation (He et al., 2017).

In summary, we have demonstrated a markedly changed spatial coherence between tropical land temperature variations to have occurred, and which has become increasingly synchronized over the past six decades. Data- and mechanistic model-based evidence suggest that the degree of spatial coherence in temperature variation is likely to be at least partially linked to features of Pacific SSTs. Our findings have significant implications for research in the global carbon cycle, climate change impacts and adaptations, and the development of climate policy. For instance, since coherence implies less spatial compensation (Figures 1 and S15), increased spatial temperature coherence might also partly explain recent

raised carbon-cycle sensitivity to tropical land temperature (Wang et al., 2014). The enhanced spatial coherence of temperature fluctuations may lead to increased risks of co-occurrences of temperature extremes across larger geographical ranges. This is especially important, when considered as an addition to more general background global warming. Raised temperature coherence could result in unprecedented detrimental simultaneous impacts on ecosystem services and the welfare of human society.

Acknowledgments

We acknowledge the World Climate Research Programme's Working Group on Coupled Modeling, which is responsible for CMIP, and we thank the climate modeling groups for producing and making available their model output. This study was supported by the National Natural Science Foundation of China (41530528), National Youth Top-notch Talent Support Program in China, and the 111 Project (B14001). C. H. recognizes the NERC CEH National Capability fund. J. Z. acknowledges funding from the Swiss National Science Foundation (PZ00P2_179876). No competing interests were declared. All data used in this study are freely available online, as listed in Table S4.

References

- Arthur, D., & Vassilvitskii, S. (2007). k-means++: The advantages of careful seeding. In *Proceedings of the eighteenth annual ACM-SIAM symposium on Discrete algorithms, Society for Industrial and Applied Mathematics* (pp. 1027-1035).
- Battisti, D. S., & Naylor, R. I. (2009). Historical warnings of future food insecurity with unprecedented seasonal heat. *Science*, 323(5911), 240–244. <https://doi.org/10.1126/science.1164363>
- Bellenger, H., Guilyardi, E., Leloup, J., Lengaigne, M., & Vialard, J. (2014). ENSO representation in climate models: From CMIP3 to CMIP5. *Climate Dynamics*, 42(7-8), 1999–2018. <https://doi.org/10.1007/s00382-013-1783-z>
- Chavez, E., Conway, G., Ghil, M., & Sadler, M. (2015). An end-to-end assessment of extreme weather impacts on food security. *Nature Climate Change*, 5(11), 997–1001. <https://doi.org/10.1038/nclimate2747>
- Christensen, J. H., Krishna Kumar, K., Aldrian, E., An, S.-I., Cavalcanti, I. F. A., de Castro, M., Dong, W., et al. (2013). Climate phenomena and their relevance for future regional climate change. In T. F. Stocker et al. (Eds.), *Climate change 2013: The physical science basis. Contribution of Working Group I to the Fifth Assessment Report of the Intergovernmental Panel on Climate Change* (pp. 1253–1255). Cambridge, UK and New York: Cambridge University Press.
- D'Arrigo, R., Wilson, R., Deser, C., Wiles, G., Cook, E., Villalba, R., et al. (2005). Tropical-North Pacific climate linkages over the past four centuries. *Journal of Climate*, 18(24), 5253–5265. <https://doi.org/10.1175/JCLI3602.1>
- Dong, B., & Lu, R. (2013). Interdecadal enhancement of the walker circulation over the tropical Pacific in the late 1990s. *Advances in Atmospheric Sciences*, 30(2), 247–262. <https://doi.org/10.1007/s00376-012-2069-9>
- Evans, M. N., Cane, M. A., Schrag, D. P., Kaplan, A., Linsley, B. K., Villalba, R., & Wellington, G. M. (2001). Support for tropically-driven Pacific decadal variability based on paleoproxy evidence. *Geophysical Research Letters*, 28(19), 3689–3692. <https://doi.org/10.1029/2001GL013223>
- Farneti, R. (2017). Modelling interdecadal climate variability and the role of the ocean. *Wiley Interdisciplinary Reviews: Climate Change*, 8(1), e441. <https://doi.org/10.1002/wcc.441>
- Harris, I. P. D. J., Jones, P. D., Osborn, T. J., & Lister, D. H. (2014). Updated high-resolution grids of monthly climatic observations-the CRU TS3.10 dataset. *International Journal of Climatology*, 34(3), 623–642. <https://doi.org/10.1002/joc.3711>
- Hazeleger, W., Severijns, C., Seager, R., & Molteni, F. (2005). Tropical Pacific-driven decadal energy transport variability. *Journal of Climate*, 18(12), 2037–2051. <https://doi.org/10.1175/JCLI3389.1>
- He, J., Deser, C., & Soden, B. J. (2017). Atmospheric and oceanic origins of tropical precipitation variability. *Journal of Climate*, 30(9), 3197–3217. <https://doi.org/10.1175/JCLI-D-16-0714.1>
- Huntingford, C., Jones, P. D., Livina, V. N., Lenton, T. M., & Cox, P. M. (2013). No increase in global temperature variability despite changing regional patterns. *Nature*, 500(7462), 327–330. <https://doi.org/10.1038/nature12310>
- IPCC (2012). In C. B. Field et al. (Eds.), *Managing the risks of extreme events and disasters to advance climate change adaptation. A Special Report of Working Groups I and II of the Intergovernmental Panel on Climate Change*. Cambridge, UK and New York: Cambridge University Press.
- Julian, P. R., & Chervin, R. M. (1978). A study of the Southern Oscillation and Walker circulation phenomenon. *Monthly Weather Review*, 106(10), 1433–1451. [https://doi.org/10.1175/1520-0493\(1978\)106<1433:ASOTSO>2.0.CO;2](https://doi.org/10.1175/1520-0493(1978)106<1433:ASOTSO>2.0.CO;2)
- Kalnay, E., Kanamitsu, M., Kistler, R., Collins, W., Deaven, D., Gandin, L., et al. (1996). The NCEP/NCAR 40-year reanalysis project. *Bulletin of the American Meteorological Society*, 77(3), 437–471. [https://doi.org/10.1175/1520-0477\(1996\)077<0437:TYNRP>2.0.CO;2](https://doi.org/10.1175/1520-0477(1996)077<0437:TYNRP>2.0.CO;2)
- Liu, Z., & Alexander, M. (2007). Atmospheric bridge, oceanic tunnel, and global climatic teleconnections. *Reviews of Geophysics*, 45, RG2005. <https://doi.org/10.1029/2005RG000172>
- Mantua, N. J., & Hare, S. R. (2002). The Pacific decadal oscillation. *Journal of Oceanography*, 58(1), 35–44. <https://doi.org/10.1023/A:1015820616384>
- Mantua, N. J., Hare, S. R., Zhang, Y., Wallace, J. M., & Francis, R. C. (1997). A Pacific interdecadal climate oscillation with impacts on salmon production. *Bulletin of the American Meteorological Society*, 78(6), 1069–1079. [https://doi.org/10.1175/1520-0477\(1997\)078<1069:APICOW>2.0.CO;2](https://doi.org/10.1175/1520-0477(1997)078<1069:APICOW>2.0.CO;2)
- Meehl, G. A., & Claudia, T. (2004). More intense, more frequent, and longer lasting heat waves in the 21st century. *Science*, 305(5686), 994–997. <https://doi.org/10.1126/science.1098704>
- Miller, A. J., & Schneider, N. (2000). Interdecadal climate regime dynamics in the North Pacific Ocean: Theories, observations and ecosystem impacts. *Progress in Oceanography*, 47(2–4), 355–379. [https://doi.org/10.1016/S0079-6611\(00\)00044-6](https://doi.org/10.1016/S0079-6611(00)00044-6)
- Mitchell, T. D., & Jones, P. D. (2005). An improved method of constructing a database of monthly climate observations and associated high-resolution grids. *International Journal of Climatology*, 25(6), 693–712. <https://doi.org/10.1002/joc.1181>
- New, M., Hulme, M., & Jones, P. (1999). Representing twentieth-century space-time climate variability. Part I: Development of a 1961–90 mean monthly terrestrial climatology. *Journal of Climate*, 12(3), 829–856. [https://doi.org/10.1175/1520-0442\(1999\)012<0829:RTCSTC>2.0.CO;2](https://doi.org/10.1175/1520-0442(1999)012<0829:RTCSTC>2.0.CO;2)
- New, M., Hulme, M., & Jones, P. (2000). Representing twentieth-century space-time climate variability. Part II: Development of 1901–96 monthly grids of terrestrial surface climate. *Journal of Climate*, 13(13), 2217–2238. [https://doi.org/10.1175/1520-0442\(2000\)013<2217:RTCSTC>2.0.CO;2](https://doi.org/10.1175/1520-0442(2000)013<2217:RTCSTC>2.0.CO;2)
- Newman, M., Alexander, M. A., Ault, T. R., Cobb, K. M., Deser, C., di Lorenzo, E., et al. (2016). The Pacific decadal oscillation, revisited. *Journal of Climate*, 29(12), 4399–4427. <https://doi.org/10.1175/JCLI-D-15-0508.1>
- Poli, P., Hersbach, H., Dee, D. P., Berrisford, P., Simmons, A. J., Vitart, F., et al. (2016). ERA-20C: An atmospheric reanalysis of the twentieth century. *Journal of Climate*, 29(11), 4083–4097. <https://doi.org/10.1175/JCLI-D-15-0556.1>
- Rahmstorf, S., & Coumou, D. (2011). Increase of extreme events in a warming world. *Proceedings of the National Academy of Sciences of the United States of America*, 108(44), 17,905–17,909. <https://doi.org/10.1073/pnas.1101766108>

- Rayner, N. A., Parker, D. E., Horton, E. B., Folland, C. K., Alexander, L. V., Rowell, D. P., et al. (2003). Global analyses of sea surface temperature, sea ice, and night marine air temperature since the late nineteenth century. *Journal of Geophysical Research*, *108*(D14), 4407. <https://doi.org/10.1029/2002JD002670>
- Rodionov, S. N. (2004). A sequential algorithm for testing climate regime shifts. *Geophysical Research Letters*, *31*, L09204. <https://doi.org/10.1029/2004GL019448>
- Rohde, R., Muller, R., Jacobsen, R., Perlmutter, S., Rosenfeld, A., Wurtele, J., et al. (2013). Berkeley earth temperature averaging process. *Geoinformatics & Geostatistics: An Overview*, *13*, 20–100.
- Taylor, K. E., Stouffer, R. J., & Meehl, G. A. (2012). An overview of CMIP5 and the experiment design. *Bulletin of the American Meteorological Society*, *93*(4), 485–498. <https://doi.org/10.1175/BAMS-D-11-00094.1>
- Trenberth, K. E. (1997). The definition of El Niño. *Bulletin of the American Meteorological Society*, *78*(12), 2771–2777. [https://doi.org/10.1175/1520-0477\(1997\)078<2771:TDOENO>2.0.CO;2](https://doi.org/10.1175/1520-0477(1997)078<2771:TDOENO>2.0.CO;2)
- Wang, X., Piao, S., Ciais, P., Friedlingstein, P., Myneni, R. B., Cox, P., et al. (2014). A two-fold increase of carbon cycle sensitivity to tropical temperature variations. *Nature*, *506*(7487), 212–215. <https://doi.org/10.1038/nature12915>
- Wilhelmi, O. V., Purvis, K. L., & Harriss, R. C. (2004). Designing a geospatial information infrastructure for mitigation of heat wave hazards in urban areas. *Natural Hazards Review*, *5*(3), 147–158. [https://doi.org/10.1061/\(ASCE\)1527-6988\(2004\)5:3\(147\)](https://doi.org/10.1061/(ASCE)1527-6988(2004)5:3(147))
- Yeh, S. W., Kang, Y. J., Noh, Y., & Miller, A. J. (2011). The North Pacific climate transitions of the winters of 1976/77 and 1988/89. *Journal of Climate*, *24*(4), 1170–1183. <https://doi.org/10.1175/2010JCLI3325.1>
- Zhang, Y., Wallace, J. M., & Battisti, D. S. (1997). ENSO-like interdecadal variability: 1900–93. *Journal of Climate*, *10*(5), 1004–1020. [https://doi.org/10.1175/1520-0442\(1997\)010<1004:ELIV>2.0.CO;2](https://doi.org/10.1175/1520-0442(1997)010<1004:ELIV>2.0.CO;2)